TEM characterisation of near surface deformation resulting from lubricated sliding wear of aluminium alloy and composites

J.C.Walker[a]*, I.M.Ross[a], W.M.Rainforth[a], M. Lieblich[b]

[a]Department of Engineering Materials, University of Sheffield, UK
[b]CENIM, Madrid, Spain

*j.walker@sheffield.ac.uk

Abstract

Aluminium alloy composites have been extensively investigated for use in tribo-contact applications, however little detailed literature exists on the sub-surface microstructural evolution as a result of lubricated sliding wear. In this study two un-reinforced alloys (2124 & 5056) and identical alloy composites, reinforced with 15vol.% $MoSi_2$ intermetallic particles were produced by a powder metallurgy route and subject to lubricated sliding at initial Hertzian contact pressures of 0.9-1.2GPa. Focused ion beam (FIB) techniques were used to produce thin sections parallel to the worn surface. Sub-surfaces layers were then examined in detail by transmission electron microscopy (TEM). Results indicated that the depth of deformation was minimal in the alloys, with the most highly deformed polycrystalline layer confined to approximately 1µm below the worn surface. Equiaxed sub-grain sizes of around 0.1µm were comparable to that observed for dry sliding of similar alloys and composites [1]. Evidence of surface erosion by solid particle impact was also observed, with wear debris generated as a result of material exceeding the ductility limit. For the composites, the $MoSi_2$ provided a suitable means of transferring the normal contact load from asperity contacts to areas in the bulk of the sample. Reinforcement fracture was observed both at the worn surface and in areas further away in the bulk, for particles which were in direct contact with each other. Evidence of the deformation of the aluminium matrix below reinforcements was also present, with average sub-grain sizes of around 330nm. Thus

such intermetallic reinforcements may have potential to replace reinforcements that are more abrasive to counterfaces, such as SiC or Al_2O_3, whilst still providing adequate wear resistance for the aluminium alloy.

Keywords: Transmission electron microscopy, aluminium composites, focused ion beam, lubricated sliding.

1 Introduction

Investigation into aluminium based metal matrix composites (MMCs) as light-weight materials for wear resistant components continues. Fundamental to this approach is the understanding of the microstructural evolution during sliding wear, which determines the wear resistance of a material under steady-state sliding conditions. Extensive studies into the characteristics of regions below the worn surfaces of ductile metals have indicated the high level of strain which is often observed as the result of sliding wear [2-7]. A fine-grained polycrystalline or sub-grain structure has been reported to occur under many conditions of sliding contact, when the stresses are sufficient to produce plastic deformation [8].

Although studies exist into the sub-surface structural evolution as the result of wear of some aluminium based composites [9-12], they are mainly confined to dry sliding, for which mechanistic differences in asperity interaction (e.g. the formation of mechanically mixed or oxide layers) exist compared to fluid film lubricated sliding. Indeed relatively few studies have investigated the lubricated sliding response of aluminium based MMCs [13-16], especially in regard to the sub-surface microstructure [1], which may be considered the most likely tribo-contact environment.

Dry sliding studies of ceramic reinforced composites indicate that load transfer between particles and matrix plays a fundamental role in the effectiveness of the composite's wear resistance. As such, the depth of deformation is often increased for MMCs, with the matrix strain between particles similar to that seen for un-reinforced alloys [1, 7, 12]. Composite wear resistance is often compromised when particle de-bonding or fracture occurs, especially where high contact stresses are involved [17].

Most of the research towards wear resistant aluminium alloy MMCs is dedicated to ceramic reinforced composites [18, 19]. However, more recently, a group of composites have emerged reinforced with intermetallic particles like $MoSi_2$ [20, 21]. Such materials are designed to retain the advantages of a harder, stiffer reinforcement phase, but be less abrasive to the counter surface.

The present investigation seeks to determine and compare the sub-surface microstructure of two aluminium alloys (2124 and 5056) reinforced by $MoSi_2$ particles, after lubricated sliding wear against an M2 tool steel counterface. Previous work [21] had indicated that at high contact stresses, a $MoSi_2$ composite provided an equal or better wear resistance than a conventional SiC reinforced alloy. Samples from the worn surface were prepared for extensive transmission electron microscopy (TEM) analysis using focused ion beam (FIB) techniques and comparisons between samples made.

2 Experimental procedure

Aluminium alloys of 2124, 5056 and metal matrix composites of these alloys, reinforced with nominally 15vol.% $MoSi_2$ particles were produced by a powder metallurgy/extrusion process and subject to lubricated sliding wear test, the details of which are given elsewhere [11, 20, 21], but summarised as follows.

Aluminium alloy powders with a mean particle size of 28μm were obtained by argon atomisation from Alpoco, UK and individually blended with 15vol.% $MoSi_2$ particles produced by self-propagating high temperature synthesis (SHS) and jet milled to a mean particle size of 5μm by INASMET, Spain. Hot extrusion of both composites and un-reinforced alloys was undertaken at extrusion ratios of 77:1 and 30:1 respectively, at 400-450ºC by Creuzet, France.

Lubricated sliding wear tests were carried out in a pin-on-ring configuration against a crowned M2 tool steel counterface rotating at $0.94ms^{-1}$. A synthetic SAE 15W-50 lubricant was used in an oil bath which the rotating counterface dipped into. Pin specimens and counterfaces were polished to <0.2μm R_a and a normal load of 630N applied, corresponding to initial Hertzian contact pressures of 0.9GPa for the un-reinforced alloys and 1.2GPa for composites. Tests were run for sliding distances greater than 350km with specific wear rates of the composites of the order $1\times10^{-10}mm^3(Nm)^{-1}$, more than half that of the un-reinforced alloys.

In order to investigate the sub-surface structural evolution as a result of the wear process, cross sectional TEM samples were prepared from each specimen using FIB techniques. Two approaches were taken; the H-bar technique as well as the external lift-out method [22]. A Jeol 6500*Fabrika* dual beam instrument was utilised which consisted of a field emission gun (FEG) SEM, coupled with an Orsay Physics ion column, attached at an incident angle of 35º to the electron beam. A liquid gallium source was used to emit Ga^+ ions at an accelerating voltage of 30kV and beam current of 1.5μA. A series of variable sized apertures allowed control of the probe current over the range ~40pA-1nA, using Canon 31 Mplus software. Elphy Quantum software from Raith allowed accurate rastering of the beam over the sample surface to sputter desired regions of material or allow deposition of Pt metal or SiO_2 from precursor gases.

The H-bar technique was used to prepare TEM samples from the 5056 alloy and 2124 + $MoSi_2$ composite, parallel to the sliding direction. The worn surface was first protected with a layer of nickel, by immersing for 1 hour in an aqueous solution containing 15 and 8% of Nickelmerse MR Electroless^{TM} (parts A and B, respectively). The solution was heated to 75ºC for an approximate 8µm thick deposition. Sectioning of the wear scars parallel to the sliding direction was then undertaken using a Streuers Accumom-7 abrasive wheel, at a slow rotation and low feed force, with copious water-based lubrication to minimise frictional heating. The samples were wax mounted on a Gatan hand-grinder and ground to less than 100µm thickness using wet 1200 SiC paper. The foil was then mounted on a 3mm half copper TEM ring using epoxy resin and attached to a suitable FIB sample holder using a carbon sticky pad. A region close to the centre of the wear scar was selected and boxes milled from both edges using a probe current of ~1nA. As the thickness of the sample approached 1µm the probe current was reduced to 250pA and finally 50pA for fine polishing of the surface.

For preparation of site-specific TEM samples, as applied to the worn surfaces of the 2124 alloy and 5056 + $MoSi_2$ composite, the external lift-out method was utilised. In order to protect the worn surface from ion interactions, deposition of either a SiO_2 layer in the case of the 2124 alloy or a Pt metal coating in the case of the 5056 + $MoSi_2$ sample from precursor gases was carried out, resulting in a layer approximately 10µm in length and 1.5µm in width and height. Wedges were milled at 45º to the surface, each side of the Pt deposit, using a probe current of ~250pA. As electron transparency was approached, final thinning was again carried out using a smaller beam current (~50pA), with a higher line repeat used to reduce re-deposition of sputtered material. Immediately prior to extraction, the sample was cut from the surrounding material. External extraction utilised a static charge on a very thin glass needle, prepared by a Narishige microelectrode puller, to attract the sample. An Olympus BH light

microscope allowed manipulation of the sample directly onto a copper based holey carbon TEM grid.

Characterisation of the samples was carried out using FEI Tecnai 20 and Jeol 2010F TEMs, both operating at 200kV and a FEI EM420 operating at 120kV. Conventional bright and dark field TEM images were taken of both the extreme worn surface as well as areas further towards the bulk of the test specimen. In addition bright field and high angle annular dark field (HAADF) scanning transmission electron microscope (STEM) images were obtained from specific regions of the 2124 + $MoSi_2$ sample. This latter technique is useful as the predominant contrast mechanism is proportional to the average atomic number. Selected area diffraction patterns as well EDX analysis allowed the interpretation of the nature of the aluminium matrix at the worn surface and the inter-relation with the $MoSi_2$ particles in the case of the composites.

3 Results

3.1 2124 Alloy

Figure 1 a) shows a secondary electron image of the worn 2124 alloy surface after lubricated sliding at 630N normal load for 469km. Trenches milled using the FIB to investigate sub-surface deformation using the ion-channelling contrast effect [21, 22] were evident parallel and perpendicular to the sliding direction. A protective layer of SiO_2 was deposited as indicated by the dashed line in a), enabling the creation of a TEM specimen by milling the reverse side, as shown in b). Sample thickness was below 200nm. Bowing of the specimen due to internal residual stresses made final thinning difficult and also resulted in the partial

removal of the protective SiO_2 deposit as can be seen in the bright field TEM micrograph, Figure 2 a), to the left of the image.

Apparent is the strain of features towards the sliding direction, up to a depth of ~4μm from the worn surface. The extreme worn surface was an uneven mixture of fine equiaxed sub-grains and larger debris particles which had become embedded in the surface, Figure 3. The average sub-grain size, taken just below the worn surface was 102 ± 15nm, Table 1, while the selected area diffraction pattern of this area gave a spotty ring appearance, showing a range of crystallographic orientations, Figure 2. Below this highly deformed layer were grains elongated towards the sliding direction, with aspect ratios of approximately 2-3. Beyond approximately 3μm depth, larger equiaxed grains consistent with the bulk grain size [21] were observed, although those nearer the worn surface exhibited a higher dislocation density and grain rotation. The high angle annular dark field TEM image in Figure 3 b) also indicated the presence of large (up to 1μm) precipitates, which EDX analysis indicated were rich in Al, with smaller amounts of Cu and Mg, as well as smaller, finer particles which EDX analysis indicated contained Al, Cu and Mn.

3.2 5056 Alloy

Figure 4 a) shows the typical worn surface of the 5056 alloy after lubricated sliding, composed of abrasive wear tracks and heavily indented surface regions. Figure 4 b) showed an SEI image of the prepared H-bar TEM sample after milling with the FIB. The high contrast electron transparent region can be seen, above which the protective nickel layer was still present. Bright field TEM, Figure 5, revealed a heavily deformed near surface region, approximately 1μm in depth, similar to the 2124 alloy, although with a distinct lack of directionality regarding the strain of surface features towards the sliding direction. Features

of the worn sub-surface included a large crater like recess (left) and sub-surface void (right). At depths of greater than approximately 3µm, un-deformed equiaxed grains were observed, again similar to the 2124 alloy.

Above the worn surface, three other types of trapped particle were observed within the nickel coating, labelled A-C in the bright field TEM montage shown in Figure 6. EDX spectra, A-C indicated that the black particles at A were rich in Fe and Cr and were therefore debris from the M2 tool steel counterface. The Ni peak could be attributed to either Ni plating or Ni also from the counterface. The spectrum from the fine grained particle B was typical of a signal from the matrix, with a large Al peak accompanied by smaller Mg and Si peaks from the alloying elements. The small Ga signal also observed was indicative of the implantation of Ga^+ ions which often occurs when manufacturing TEM specimens by this technique. The large grey particle at point C was predominantly composed of silicon and oxygen, although a small carbon peak was also observed, and could be trapped lubricant residue. Significantly, the upper contact surface appeared to be coated in a thin (~10nm) film, believed to be a boundary lubricant, which was quite distinct in Figure 7 a), appearing thicker at the base of the crater.

Grain sizes appeared to vary according to the local worn surface morphology and not necessarily as a function of depth below the worn surface. Such an example was the peak of the crater in Figure 7 a). The raised lip had a very fine grain size, whilst dark field imaging of the (311) diffraction spot showed grains with a high aspect ratio of around 7 at the base of the crater, suggesting plastic deformation by hard particle impact with significant force.

Bright field imaging of the region to the upper-right of the sub-surface void, Figure 8, indicated that there was a clear interface in the matrix. A fine grain size, similar to that observed for the debris particle at B, interspersed with voids indicated that the surface to the left in this image was in fact 5056 alloy debris which had re-adhered to the matrix, resulting

in an open pocket below the worn surface. Indeed, inspection of the grain size at the base of the large void, Figure 7 b), showed that it was finer than that immediately above it, closer to the worn surface. Dark field imaging of the (200) diffraction spot in this vicinity revealed average sub-grain sizes of 103 ± 20nm, Table 1. The void itself appeared to contain a fluid film, again attributed to remnant lubricant.

3.3 2124 + $MoSi_2$

Figure 9 was a secondary electron image of the prepared H-bar section from the worn 2124 + $MoSi_2$ sample surface. Due to residual stresses, the sample again bowed as the thickness was reduced, ultimately resulting in the preferential removal of material from the centre of the specimen, and unfortunately removing a small proportion of the worn surface. As such analysis was carried out in areas away from this area, Figures 10-12.

The most striking difference in comparison to the worn surfaces was that very little surface deformation of the aluminium matrix was observed. Equiaxed grains approximately 1µm in size were observed very close to the sample surface, Figure 10, with a high apparent dislocation density, but no evidence of the formation of an elongated cell structure. Figure 11 a) and b) compare STEM bright and high angle annular dark field images of the worn surface where a series of $MoSi_2$ particles, which appeared with high contrast in the HAADF images, b) and c), extended into the bulk, as can also be seen in Figure 9. Apparent was the detachment of the protective Ni surface layer from the upper $MoSi_2$ particle, which occurred during sample preparation. EDX analysis of the particle labelled A which appeared embedded in the sample surface, Figure 12, indicated that it was mixture of Al and Fe, suggesting the wear debris had become embedded in the worn surface.

Significantly, the reinforcement particle labelled B further from the worn surface, confirmed as $MoSi_2$ from the EDX trace shown in Figure 12, showed signs of fracture whilst the one at the contact surface did not. This was indeed the case as can be seen in the magnified HAADF image in Figure 11 c), where it is clear that contact points from the upper particle were causing fracture of the lower particle. This effect also continued with reinforcement particles even further from the worn surface, Figure 11 d), which were in direct contact with each other.

3.4 5056+$MoSi_2$

Site specific investigation of the worn 5056 + $MoSi_2$ composite surface was carried out within one of the regions that exhibited ploughing, in order to determine the effect of reinforcement fracture. As such a protective Pt deposit was applied to the region indicated in Figure 13 a), almost parallel to the sliding direction. Initial thinning from one side allowed SEM examination of the worn sub-surface, Figure 13 b), which revealed both fractured reinforcements at the extreme worn surface, as well as un-fractured reinforcements within a couple of microns of the contact surface.

Milling of the reverse side of this trench also allowed the preparation of a TEM specimen, the upper thickness of which was approximately 70nm. Further thinning was again impeded by residual stresses causing bowing in the sample. As previously outlined, sample extraction utilised the static charge between sample and a glass needle and Figure 13 c) showed the TEM specimen after cutting from the worn surface, prior to pick up and deposition onto a carbon grid.

Bright field TEM images of this sample, Figures 13 d) and 14, further showed the surface fracture of the silicides, but also suggested that the total depth of deformation of the

aluminium grains was greater under the reinforcement, compared to an area when the matrix was continuous from the worn surface to the bulk. Numerous small particles, believed to be re-implanted $MoSi_2$, were observed embedded in the surface of the matrix in this region. Average sub-grain sizes, measured from below the fractured reinforcement, Figure 15 a), were 329 ± 39nm, Table 1. The central $MoSi_2$ particle was part of a larger reinforcement that extended to the worn surface, Figure 13 b). Figures 15 b) and c) clearly show an overlapping aluminium grain, the tip of which appears to be associated with dislocation pile-ups within this $MoSi_2$ particle. Indeed, deformed sub-grains below this particle are similar in size to those closer to the worn surface. Away from reinforcements, the equiaxed sub-grain structure at the worn surface exhibited minimal surface strains towards the direction of sliding, similar to the un-reinforced 5056 alloy.

4 Discussion

4.1 Un-reinforced alloys

During sample preparation it was frequently noted the effect of residual stress that resulted in bowing of the sample as the thickness was reduced. This highlighted the care that was required when using the FIB technique for these materials, which differed substantially for materials more commonly produced by this method, such as silicon [22].

As shown in Figure 1 a) and 4 a), the worn alloy surfaces where characterised by two types of surface morphology; ploughed or indented regions. The cross sectional sub-surface area for the 2124 alloy was close to an abrasive groove. Evident was the displacement of the microstructure towards the sliding direction, believed to be the result of the ductile micro-ploughing which appeared to have occurred. In contrast, the sample removed from the 5056

alloy was believed to be from a region dominated by a different type of wear mechanism. The strain of features appeared to be sensitive to local asperity deformation events, rather than towards the sliding direction and it was believed that this area was similar to that shown by the indented morphology in Figure 4 a). The large impact crater to the left of Figure 4 a) appeared to be the result of solid particle impact, perhaps by a hard particle from the counterface, given the local presence of Fe rich debris. The deformation of the local sub-surface microstructure was similar to that observed during erosive tests by solid particle impact [4, 23], where the bulk of the deformation was confined to the immediate vicinity below the impact crater and where normal contact loads are not transferred from the counterface by asperity interaction. Calculations of the minimum fluid film thickness based upon surface roughness values taken elsewhere [21, 24] indicated a partial elasto-hydrodynamic fluid film thickness of less than a micron was to be expected. For larger debris particles this would result in abrasive wear as the normal load would be transferred through the debris particle to the surface. However, for smaller particles trapped in the lubricant as it flowed through the contact area, erosive wear, perhaps similar to small scale slurry erosion would take place, although this would have a lesser effect in terms of wear of the sample surface compared to ductile microploughing.

Equiaxed sub-grains were observed in both alloys, usually at the worn surface, or associated with debris particles that had become embedded in the protective Ni layer, Figures 3 b), 7 and 8. This was evidence of the primary material removal mechanism from the worn surface, where the ductility limit of the alloy had been reached and material was removed as wear debris. One exception was shown in Figure 7 b) where the minimum sub-grain size occurred below the worn surface. This type of behaviour has previously been noted for dry sliding wear of similar alloys [1, 4],where dynamic recrystallisation had occurred at the worn contact surface as the result of local flash temperatures. However, this was not considered to

be the case in this particular instance. Rather, the re-adherence of removed aluminium debris to the worn alloy surface was considered more appropriate, evidence of which was trapped lubricant in the large void that was created below the worn surface as a result of the debris adhesion, Figure 7 b), as well as the obvious interface between such transferred material and the former worn surface, Figure 8 Whilst contact stresses would be at their highest below the worn surface, as this part of the sample was considered to be from an eroded surface, the nucleation of sub-surface voids, especially those the size of that in Figure 6 was not considered to be feasible under such contact conditions.

The sub-surface microstructure of both alloys was characterised by a heavily deformed near surface layer, approximately 1μm in depth. Selected area diffraction patterns from this region confirmed the polycrystalline nature, while average sub-grain sizes of approximately 100nm, Table 1, were common to both alloys. This was despite the presence of what was believed to be the S´ precipitates [25] as well as a fine dispersion of Al rich particles containing smaller amounts of Cu and Mn in the 2124 matrix, Figure 3 b). Such an observation is consistent with other studies [26] which suggest that small precipitates in age-hardened alloys offer relatively little benefit to the wear resistance of such alloys due to the large strains that occur. As such the wear resistance becomes more a function of the surface hardness developed due to work hardening mechanisms, rather than that of the bulk hardness due to precipitation sequences [7, 27].

Such sub-grain sizes were comparable to that observed during dry sliding of similar alloys, where it was demonstrated that minimum sub-grain sizes of around 0.2-0.4μm were achieved, irrespective of the applied load [1, 9, 16]. This was further evidence of the microstructural evolution during wear depending on the particular alloy system, regardless of contact conditions, which for wear, again, tends to be associated with the response of the material to high strains [3, 7, 27]. Compared to similar dry sliding studies [11, 28] the depth

of high strain deformation of was small, consistent with the minimal specific wear rates of the order 1×10^{-9} $mm^3(Nm)^{-1}$ observed for these materials under lubricated sliding contact [21].

4.2 $MoSi_2$ reinforced composites

At high initial Hertzian contact stresses of over 1GPa, reinforcement fracture would be expected to occur during asperity contact, and indeed evidence of $MoSi_2$ fracture was observed in both the 2124 and 5056 alloy composites. Importantly, the reinforcement remained bonded to the matrix after fracture, with no evidence of particle-pull out from the worn surface. This allowed the reinforcement to continue conferring a degree of wear resistance, as was indicated by the extended depth of deformation of the aluminium matrix below the fractured particles to the left of Figure 13 d). Both alloy composites demonstrated the ability to transfer the normal contact load through reinforcements that extended from the wear surface into the bulk, Figures 11 and 13. In the case of the 2124 + $MoSi_2$ composite, clear evidence of the fracture of reinforcements further away from the worn surface was presented in Figures 11 c) and d), whilst the reinforcement at the surface remained intact and hence acted as a load bearing asperity contact with the counterface. It appeared that the contact points from the upper particle were responsible for the stress concentration and thus crack initiation in the lower particle. For the 5056 + $MoSi_2$ composite, evidence of deformation of grains below the central reinforcement particle, Figures 15 b) and c) was again as the result of this particle extending to the worn surface, Figure 13 b), although thinning to create a TEM specimen had resulted in the upper part of the particle being removed.

The presence of debris particles rich in aluminium and iron as indicated by particle A in Figure 11 a) and 12 would suggest a degree of mixing of wear debris, as well as re-

adhesion to the worn surface, perhaps similar to that observed for the 5056 alloy surface. The Ni signal observed in EDX spectrum B, Figure 12, was attributed to resputtered material from the protective Ni layer.

One distinct difference between the composite samples and the un-reinforced alloys was the deformed grain size. The average sub-grain size for the 5056 + $MoSi_2$ composite was approximately 330μm, three times greater than for the alloys, and reflected both the reduction in matrix deformation as a result of larger, stiffer reinforcement particles, as well as the increase in relative wear resistance for the composites. However, for the 2124 + $MoSi_2$ sample, equiaxed un-deformed grains, albeit with a high dislocation density, were observed very close to the worn surface, Figure 10. Thus for this sample area the $MoSi_2$ particles were acting as excellent reinforcements, transferring the normal contact load to adjacent particles further into the bulk of the material, whilst leaving the aluminium surface un-deformed.

5 Summary

- Focused ion beam techniques have been successfully used to produce TEM samples of selected areas of the worn surface from a number of aluminium alloy and $MoSi_2$ composites, although residual stresses often caused bowing as the sample thickness was reduced to less than 200nm.
- The un-reinforced alloys both exhibited a highly deformed near surface layer, approximately 1μm in thickness, composed of equiaxed sub-grains of ~0.1μm in size, similar to that for dry sliding studies.
- The worn surface morphology after lubricated sliding was composed of ductile ploughed wear tracks, interspersed by heavily indented regions, similar in nature to an eroded surface.

- The strain of surface features was highly sensitive to the local deformation of asperities and debris generation appeared to be by material exceeding the ductility limit of the alloy.
- In contrast, the alloy composites did not exhibit a near surface deformation layer. Rather, the reinforcement effectively transferred the normal contact load to the bulk underlying structure. This resulted in either deformed equiaxed sub-grains in the aluminium matrix, or fractured reinforcement particles, depending on what lay beneath.
- Thus $MoSi_2$ has been demonstrated to be an effective reinforcement for lubricated sliding of aluminium alloys. Despite fracturing upon asperity contact, it appeared that the local bonding with the matrix enables effective load transfer, whilst simultaneously offering a less abrasive contact to the mating counterface material.

Acknowledgements

Thanks to A.Chang for assistance with FIB sample lift-out and to EPSRC (UK) for the funding of the studentship for this project.

References

[1] Perrin, C. and Rainforth, W.M., *The effect of alumina fibre reinforcement on the wear of an Al-4.3%Cu alloy,* Wear, 1995, **181-183** (1), pp. 312-324.

[2] Bowden, F.P. and Tabor, D., *The friction and lubrication of solids*, Vol. 1, 1950, Oxford University Press.

[3] Dautzenberg, J.H. and Zaat, J.H., *Quantitative determination of deformation by sliding wear,* Wear, 1973, **23**, pp. 9-19.

[4] Ives, L.K., *Microstructual changes in copper due to abrasive, dry and lubricated wear*, in Proc. *Wear of Materials*, 1979, ASME.

[5] Rigney, D.A. and Glaeser, W.A., *The significance of near surface microstructure in the wear process,* Wear, 1978, **46**, pp. 241-250.

[6] Rigney, D.A., *Large strains associated with sliding contact of metals,* Mat. Res. Innovat., 1998, **1**, pp. 231-234.

[7] Rainforth, W.M., *Microstructural evolution at the worn surface: a comparison of metals and ceramics,* Wear, 2000, **245**, pp. 162-177.

[8] Ruff, A.W., Ives, L.K., and Glaeser, W.A., *Characterisation of wear surfaces and wear debris,* in *Fundamentals of friction and wear of materials*, D.A. Rigney, Ed. 1981, ASM, Ohio, pp. 235-289.

[9] Perrin, C. and Rainforth, W.M., *Work hardening behaviour at the worn surface of Al-Cu and Al-Si alloys,* Wear, 1997, **203-204**, pp. 171-179.

[10] Wang, Y., Rainforth, W.M., Jones, H., and Lieblich, M., *Dry wear behaviour and its relation to microstructure of novel 6092 aluminium alloy-Ni_3Al powder metallury composite*, Wear, 2001, **251**, pp. 1421-1432.

[11] Wang, Y., Rainforth, W.M., Jones, H., and Lieblich, M., *Sliding wear behaviour of novel AA2124 aluminium alloy/Ni_3Al composites,* Mater. Sci. Forum, 2002, **396-402**, pp. 1473-1478.

[12] Leonard, A.J., Perrin, C., and Rainforth, W.M., *Microstructural changes induced by dry sliding wear of a A357/SiC metal matrix composite,* Mat. Sci. and Tech., 1997, **13**, pp. 41-48.

[13] Alpas, A.T. and Embury, J.D., *Slidng and abrasive wear behaviour of an aluminium (2014)-SiC particule reinforced composite,* Scripta Met. and Mat., 1990, **24**, pp. 931-935.

[14] Lin, S.J., Lin, C.A., Wu, G.A., and Hong, J.L., *Sliding wear of Al_2O_{3p}/6061 Al composite*, J. Mat. Sci., 1996, **31** (13), pp. 3481-3486.

[15] Pan, Y.M., Fine, M.E., and Cheng, H.S., *Ageing effects on the wear behaviour of P/M aluminium alloy SiC particulate composites,* Scr. Metall., 1990, **24**, pp. 1341-1345.

[16] Pan, Y.M., Fine, M.E., and Cheng, H.S., *Sliding wear of an Al alloy SiC whisker composite*, Tribol. Trans., 1992, **35** (3), pp. 482-490.

[17] Zhang, J. and Alpas, A.T., *Wear regimes and transitions in Al_2O_3 particulate - reinforced aluminium alloys,* Mater. Sci. Eng., 1993, **A161**, pp. 273-284.

[18] Deuis, R.L., Subramanian, C., and Yellup, J.M., *Dry sliding wear of aluminium composites - A review*, Comp. Sci. & Tech., 1996, **57**, pp. 415-435.

[19] Sannino, A.P. and Rack, H.J., *Dry sliding wear of discontinuously reinforced aluminium composites: review and discussion,* Wear, 1995, **189**, pp. 1-19.

[20] Torres, B., Lieblich, M., Ibanez, J., and Garcia-Escorial, A., *Mechanical properties of some PM aluminide and silicide reinforced 2124 aluminium matrix composites,* Scripta Mater., 2002, **47**, pp. 45-49.

[21] Walker, J.C., Rainforth, W.M., and Jones, H., *Lubricated sliding wear of behaviour of aluminium alloy composites,* Wear, 2005, **259**, pp. 577-589.

[22] Giannuzzi, L.A. and Stevie, F.A., *Introduction to focused ion beams*, 2004, Springer.

[23] Hutchings, I.M., *Abrasive and erosive wear of metal matrix composites (MMCs),* in Proc. *European conference on advanced materials and processes*, 1992, EuroMat '91.

[24] Walker, J.C., *Lubricated sliding wear of some aluminium alloy composites*, in *Department of Engineering Materials*, 2006, University of Sheffield, Sheffield.

[25] Smith, G.W., Baxter, W.J., and Mishra, R.K., *Precipitation in 339 and 2124 aluminium: A caveat for calorimetry,* J. Mat. Sci., 2000, **35**, pp. 3871-3880.

[26] Bhansali, K.J. and Mehrabian, R., *Abrasive wear of aluminium-matrix composites,* J. Met., 1982, **34**, pp. 30-34.

[27] Hutchings, I.M., *Tribology,* 1992, Cambridge, Butterworth-Heinemann.

[28] Ghazali, M.J., Rainforth, W.M., and Jones, H., *Dry sliding wear behaviour of some wrought, rapidly solidified powder metallurgy aluminium alloys,* Wear, 2005, **259**, pp. 490-500.

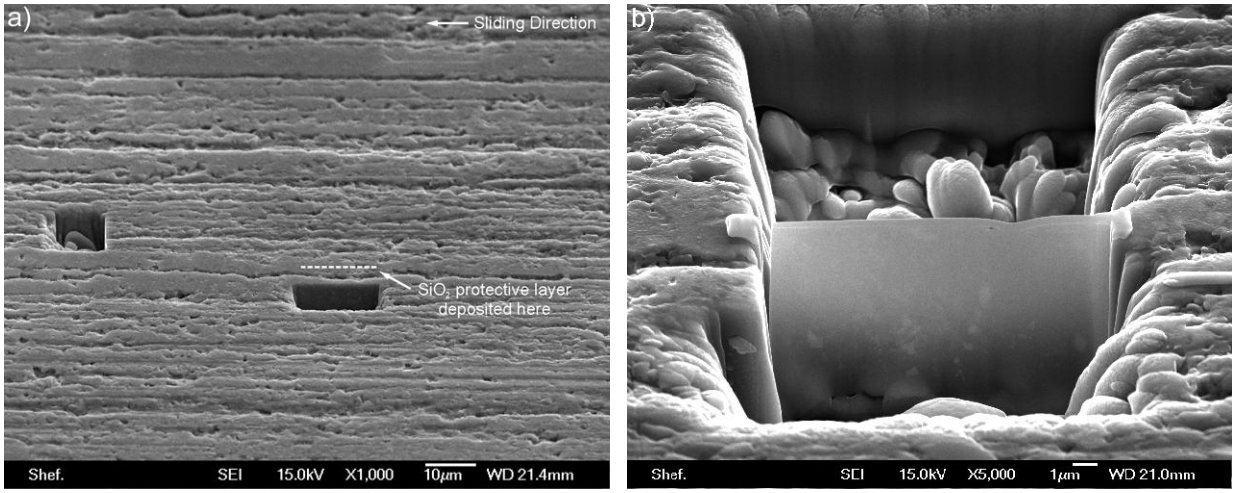

Figure 1. Secondary electron (SEI) SEM images of a) area where SiO_2 was deposited on the worn 2124 alloy surface and b) the TEM specimen of the sub-surface area, prior to final thinning and external lift-out.

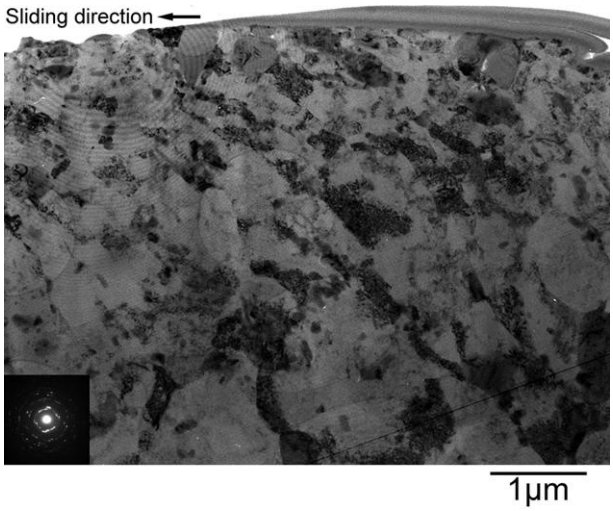

Figure 2. Bright field TEM image of worn 2124 alloy sub-surface and SADP of an area immediately below the worn surface.

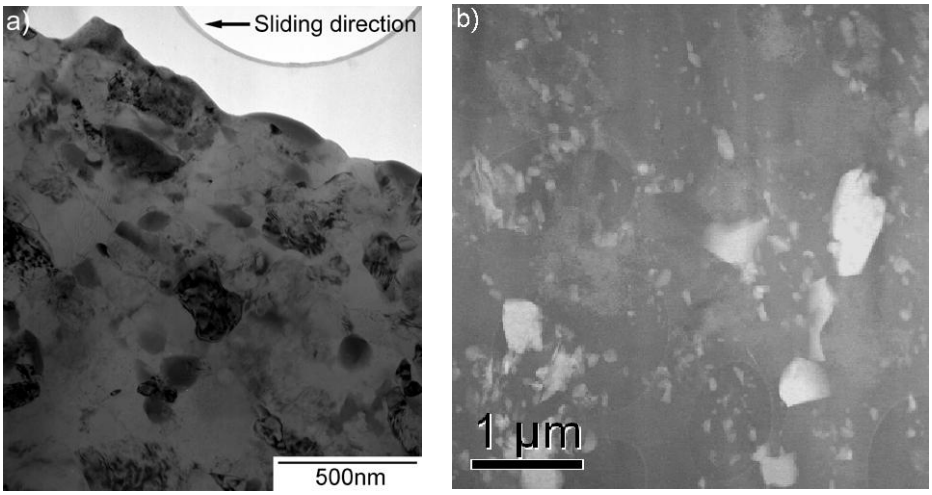

Figure 3. a) Higher magnification bright field TEM image of the extreme worn surface and b) HAADF image showing precipitates within the bulk matrix.

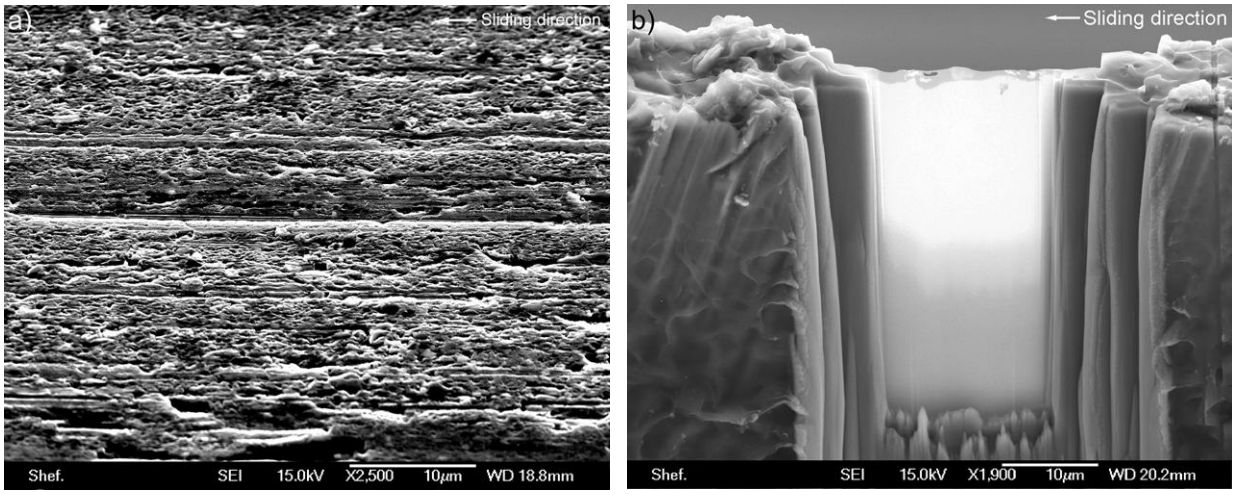

Figure 4. a) SEI image of FIB milled H-bar section of the worn 5056 alloy surface and b) corresponding bright field TEM image of the electron transparent area.

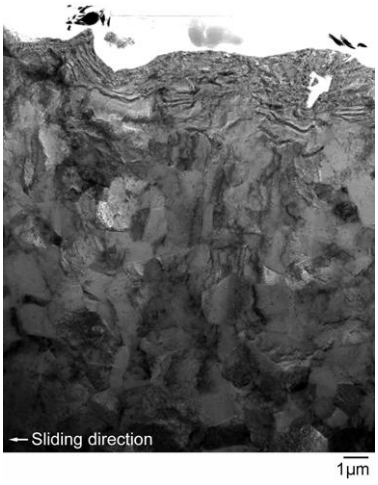

Figure 5. Bright field TEM image of the worn sub-surface area shown in Figure 4 b).

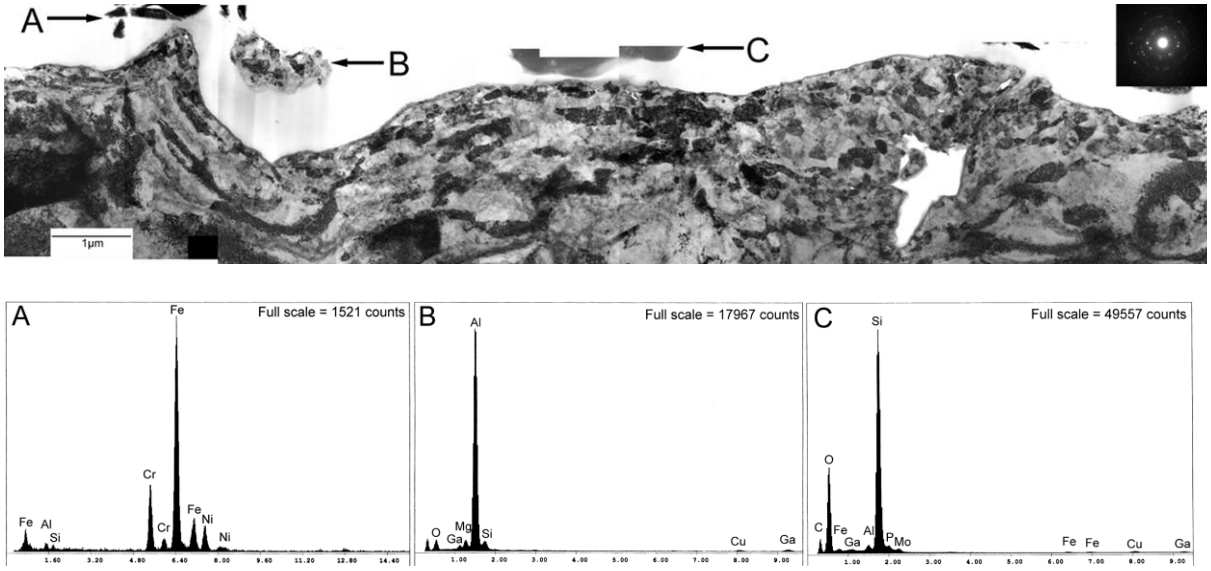

Figure 6. Bright field TEM micrograph montage of worn 5056 alloy surface. Points A-C correspond to EDX spectra indicated, whilst the selected area diffraction pattern was taken from an area just below the worn surface, to the right of particle C.

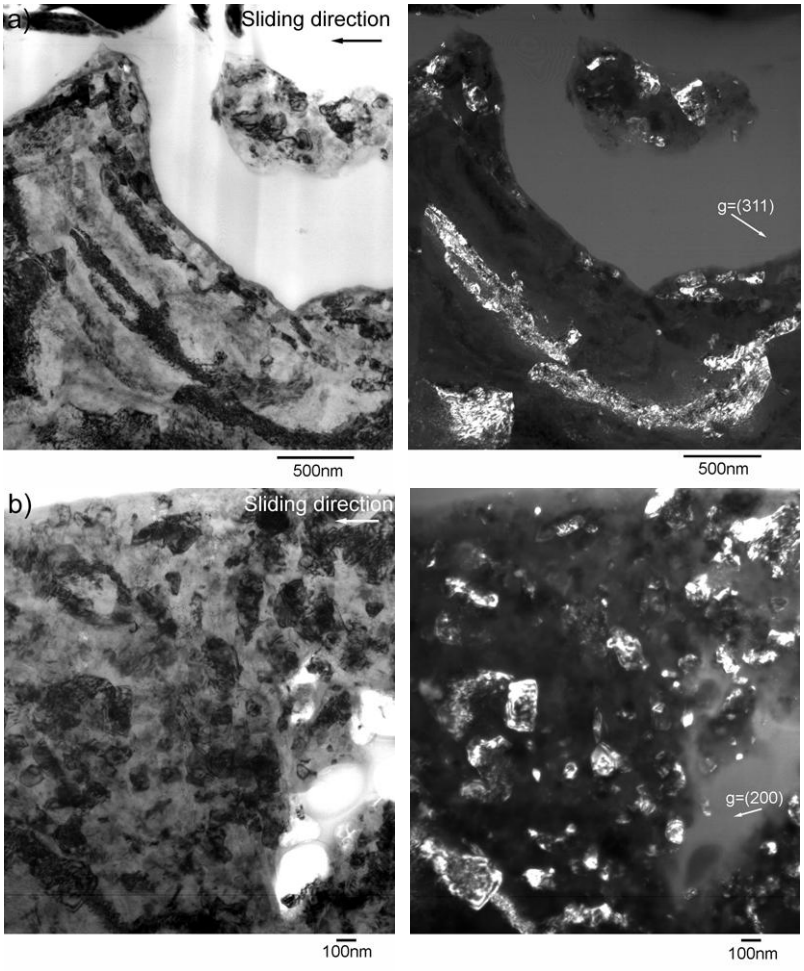

Figure 7. Bright and dark field TEM images pairs of deformed grains below a) impact crater and b) next to the sub-surface void in 5056 alloy worn surface.

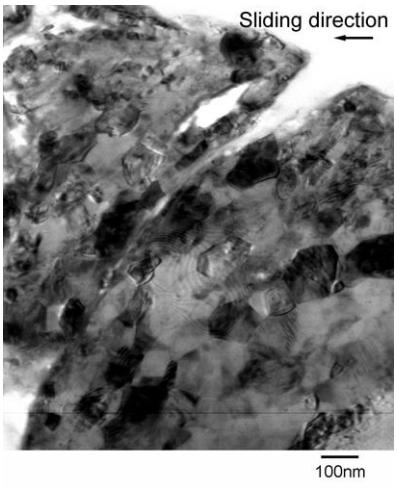

Figure 8. Bright field TEM image taken from the right of Fig. 4 showing the interface between debris (left) and worn 5056 alloy surface (right).

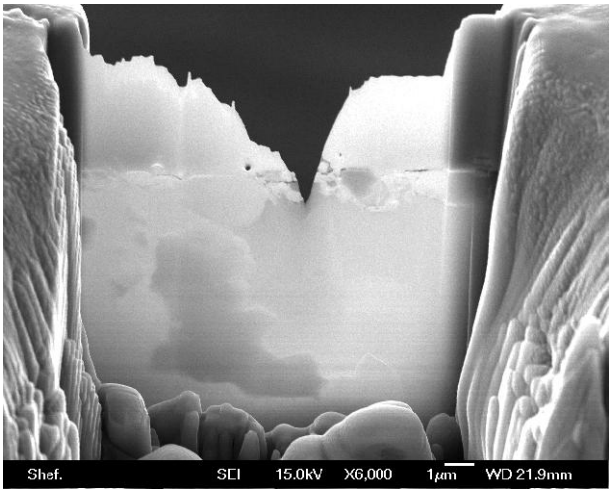

Figure 9.SEI image of H-bar FIB section through 2124 + $MoSi_2$ worn surface. The upper region is the protective Ni coating.

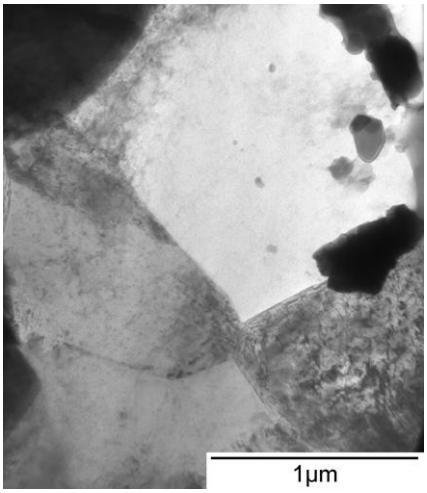

Figure 10. Bright field TEM image of equiaxed un-deformed grains near worn surface of 2124 + $MoSi_2$ composite.

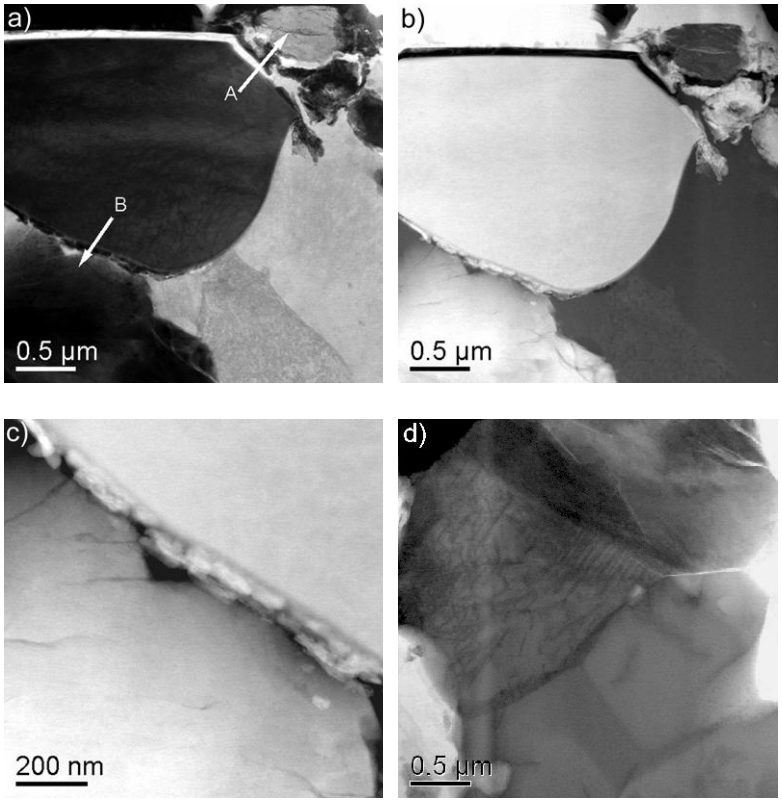

Figure 11. Bright field (a) and HAADF (b) STEM images of the worn 2124 + $MoSi_2$ sub-surface. Evident in the HAADF (c) and bright field (d) images was the fracture of the reinforcement further away from the worn surface.

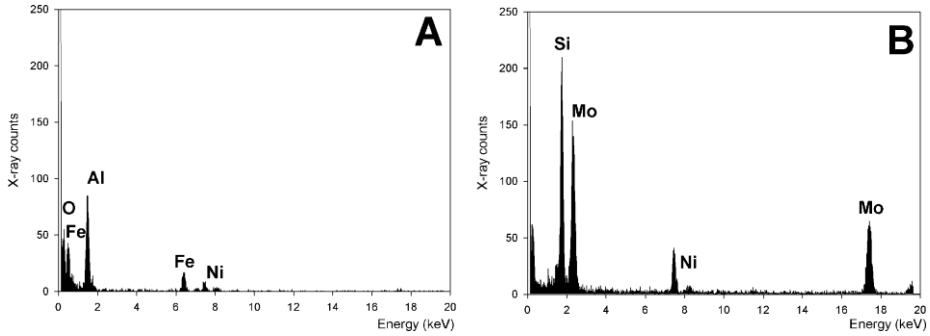

Figure 12. EDX spectra of implanted particle A, and reinforcement, B, from Fig 9 a).

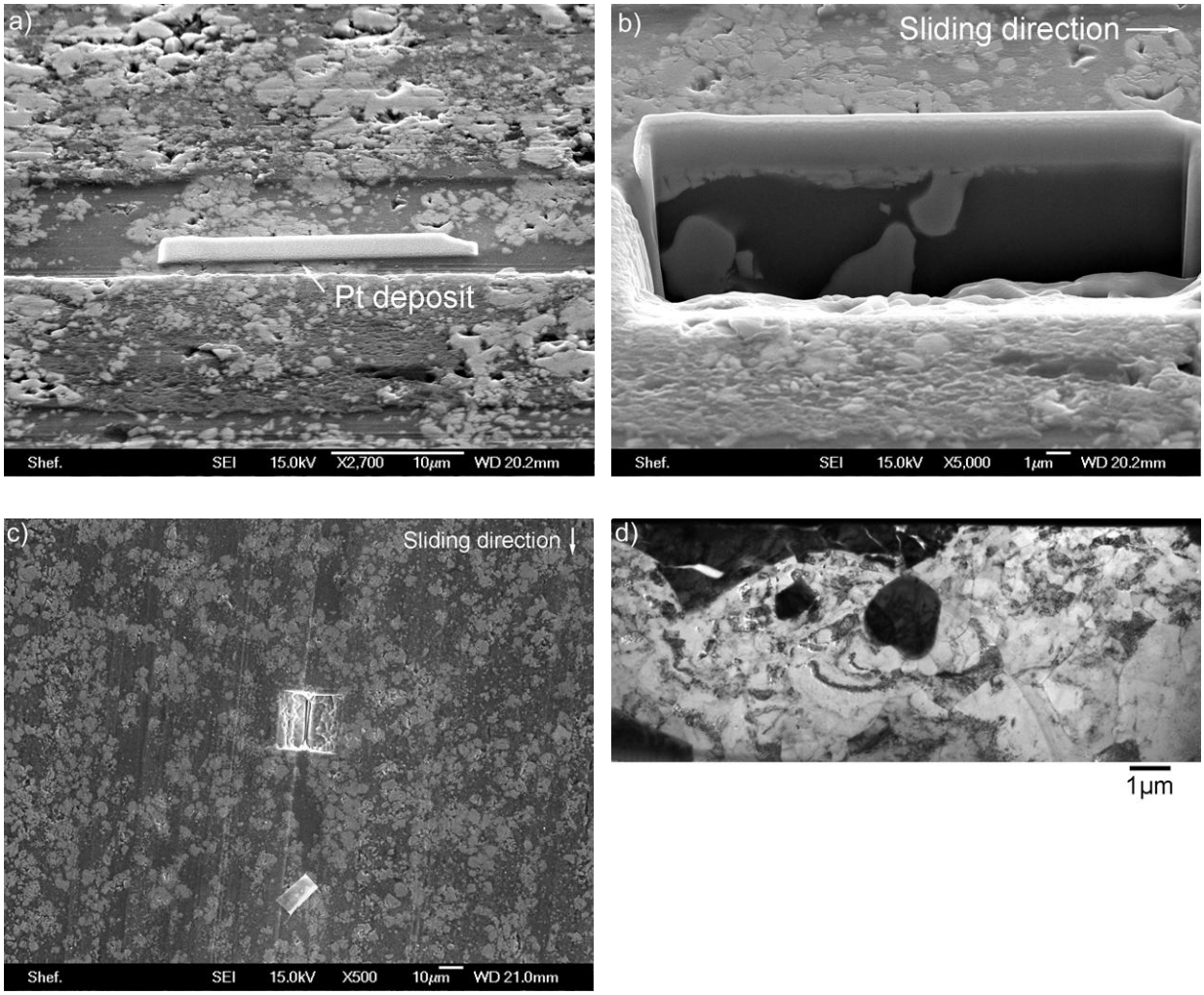

Figure 13. SEI images showing site-specific preparation of a TEM sample from the worn surface of 5056 + $MoSi_2$. a) deposition of Pt over fractured reinforcement, b) FIB sputtered trench, c) TEM sample released from nearby area of interest and d), a bright field TEM image of the same sample.

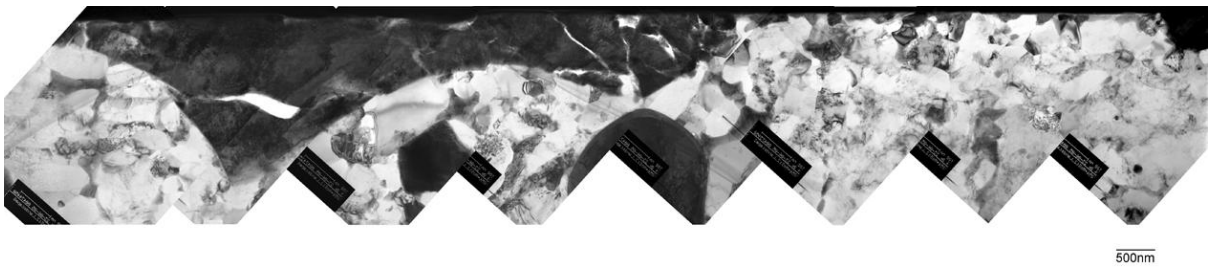

Figure 14. Bright field TEM montage of worn 5056 + $MoSi_2$ composite surface.

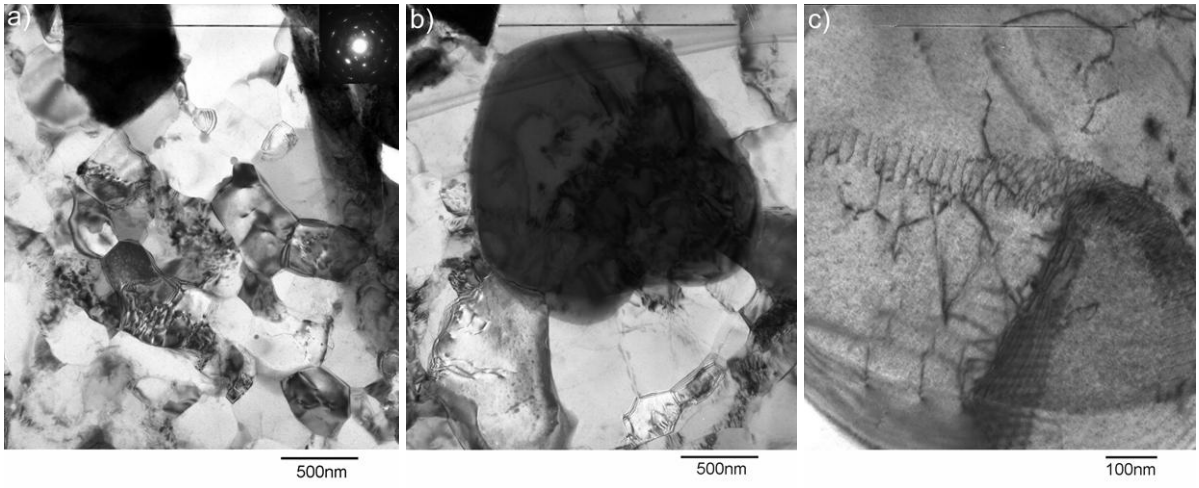

Figure 15. Bright field TEM images from worn 5056+$MoSi_2$ sub-surface, indicating a) subgrains below fractured reinforcement, b) microstructure below central reinforcing particle and c) dislocation interaction between central reinforcing particle and overlapping Al grain.